RSC Advances

PAPER

View Article Online
View Journal | View Issue

Cite this: *RSC Adv.*, 2024, **14**, 35220

An exceptional water stable terbium-based metal–organic framework for selective detection of pesticides†

Ching-Ping Liu, *[a] Ting-En Lin,[a] Jung-Chang Chiang,[a] Bo-Jhen Chen,[a] Po-Hsiu Chien,[a] Su-Ying Chien,[b] Gene-Hsiang Lee,[b] Yen-Hsiang Liu *[a] and Kuang-Lieh Lu*[ac]

A terbium-based metal–organic framework (MOF) with exceptional water stability for highly selective detection of pesticide thiamethoxam (TMX) in aqueous solution is reported. To date, most reported lanthanide metal–organic frameworks (Ln-MOFs) still exhibit poor water stability, which may limit their practical applications in bio-sensing and detecting pollutants in environmental water samples. In this work, a Tb-MOF $[Tb(BDC)_{1.5}(DEF)\cdot 0.5H_2O]_n$ (**1**, BDC = 1,4-benzene dicarboxylate, DEF = *N*,*N*-diethylformamide) was prepared by hydrothermal reactions of 1,4-benzenedicarboxylic acid with the corresponding rare earth ions of Tb^{3+}. Impressively, water stability surveys of compound **1** indicated that it maintained at least 90% of its emission intensity after storage in water for several months. This characteristic of long water stability is unusual as compared to other Ln-MOFs, making compound **1** an excellent candidate for sensing applications in the aqueous phase. In particular, the green emission of compound **1** could be quenched by the pesticide thiamethoxam (TMX), which was attributed to both the static and dynamic quenching processes based on an upward-curving Stern–Volmer plot. The quenching mechanism was speculatively attributed to the inner filter effect combined with the complex formation based on the electrostatic interaction of compound **1** and TMX, resulting in the promotion of the quenching efficiency. Finally, compound **1** was demonstrated to detect TMX in aqueous solution with rapid response and high selectivity.

Received 13th September 2024
Accepted 24th October 2024

DOI: 10.1039/d4ra06622g

rsc.li/rsc-advances

Introduction

Studies of lanthanide-based metal–organic frameworks (Ln-MOFs) have attracted great interest from researchers, not only because of their exceptional coordination properties and structural diversity[1,2] but also because of their potential applications in areas such as gas storage/separation, catalysis, sensing, ion exchange, magnetism, and photoluminescence.[2–5] Both Eu-MOFs and Tb-MOFs are commonly applied as sensors because of the strong visible luminescence of their f–f transitions in the red and green regions respectively, which are significantly altered *via* an "antenna effect" of guest ions.[6] It is known that MOFs possessing paddle-wheel-like or cluster-chain-like, rod-shaped secondary building units benefit network structure diversity, framework robustness, and porous network integrity.[7,8] Inspired by the variability of the lanthanide coordination ability, Ln-MOFs are also good candidates for the construction of cluster-chain like, rod-shaped building units for robust porous coordination networks.[9,10] With their light-emitting properties, these porous networks are potential candidates for applications related to metal-ion doping as well as solvent exchange induced luminescence tuning.[5,11]

Traditional techniques of chemical analysis, including chromatography and mass spectrometry, are not exactly convenient due to the complexity of the analytical process. However, photoluminescence is preferentially studied because of its high sensitivity, low cost, fast response and technical simplicity.[12] Considering the coordination availability of photo-activated organic ligands and luminescent lanthanide ions, Ln-MOFs can serve as optical sensors in the detection of temperature,[13] environmental pH,[14] drugs,[15] toxins,[16] and biomolecules.[17] However, most of the reported Ln-MOFs to date still have the drawback of weak water stability, which may limit their practical applications in bio-sensing and detecting pollutants in environmental water samples.[18] As a consequence, development of Ln-MOFs with high water stability for sensing purposes is of

[a]*Department of Chemistry, Fu Jen Catholic University, New Taipei City 242062, Taiwan. E-mail: 129723@mail.fju.edu.tw; 056461@mail.fju.edu.tw; kllu@gate.sinica.edu.tw*

[b]*Instrumentation Center, National Taiwan University, Taipei, 10617, Taiwan*

[c]*Institute of Chemistry, Academia Sinica, Taipei 115, Taiwan*

† Electronic supplementary information (ESI) available. CCDC 2378574. For ESI and crystallographic data in CIF or other electronic format see DOI: https://doi.org/10.1039/d4ra06622g

great importance in both conceptual advance and potential for practical use.

Nowadays, pesticides are still widely used in agriculture,[19] but pesticide residues are harmful to people, animals, and the environment, and they appear in the food chain. Given the significant importance of public health, fast and sensitive monitoring of pesticides in food, water, and soil is urgently required. Thiamethoxam (TMX) is a representative compound of neonicotinoid pesticides. Due to its high water solubility, poor biodegradability, and several adverse effects on the environment, each country has regulations related to the maximum residue limit (MRL) of TMX.[20] In our country, the MRL of TMX is even lower than 0.01 ppm. Recently, the MOF-based materials have been widely used to detect various pesticides, including glyphosate,[21–24] 2,6-dichloro-4-nitroaniline (DCN),[25–28] organophosphate pesticides (OPP),[29–32] parathion-methyl,[33–36] and nitenpyram,[37–40] but few studies have focused on sensing TMX in water.[41,42] These above examples for sensing pesticides based on MOFs are summarized in Table S1.†

As part of our ongoing efforts directed toward the design and synthesis of functional crystalline materials, we report herein on the structure, photoluminescence, and water stability of a Tb-based MOF, $[Tb(BDC)_{1.5}(DEF)\cdot 0.5H_2O]_n$ (**1**, BDC = 1,4-benzene dicarboxylate, DEF = *N*,*N*-diethylformamide) (Scheme 1). The emission of compound **1** can be efficiently quenched by TMX through both static and dynamic quenching processes. In addition, the emission of compound **1** was extremely stable in water, allowing operation of the sensing platform in the aqueous phase.

Experimental

Materials and instruments

All chemicals were purchased commercially and used as received without further purification. Elemental analyses were conducted on a 2400 CHN elemental analyzer (PerkinElmer, Waltham, MA, USA). Thermogravimetric analyses (TGA) were performed under a nitrogen atmosphere with a PerkinElmer TGA-7 TG analyzer. Powder X-ray diffraction patterns were recorded with a Bruker D2 Phaser diffractometer with Cu Kα (λ = 1.5406 Å). UV-vis absorption measurements in the solution state were obtained with a JASCO (V-670) spectrophotometer. Lifetime measurements were obtained with an EDINBURGH (FLS-920) spectrophotometer.

Preparation of $[Tb(BDC)_{1.5}(DEF)\cdot 0.5H_2O]_n$ (1)

In a 23 mL Teflon-lined stainless steel vessel, deionized water (1 mL) was added with vigorous stirring to a mixed solution of 1,4-benzenedicarboxylic acid (H_2BDC, 0.3 mmol) in DEF (3 mL) and 0.2 mmol of $Tb(NO_3)_3\cdot 5H_2O$ salts in DEF (2 mL) to produce homogenous solutions. The vessel was sealed and heated at 80 °C for 72 hours in a convection oven and slowly cooled to the room temperature over a five-day period. High quality cubic-shaped crystals of compound $[Tb(BDC)_{1.5}(DEF)\cdot 0.5H_2O]_n$ (**1**) were produced. The crystalline samples were collected, washed with fresh DEF solvent, and air-dried at room temperature. Yield: 51.5%, (25.7 mg) based on H_2BDC. Elemental analysis (EA) calculated (%) for $C_{17}H_{18}N_1O_{7.5}Tb$: C, 39.60; H, 3.52; N, 2.72. EA found (%): C, 39.65; H, 3.42; N, 2.79. FT-IR (ATR-IR): ν = 1662 (w), 1626 (m), 1579 (s), 1508 (w), 1439 (w), 1398 (vs), 1323 (w), 1299 (w), 1268 (w), 1212 (w), 1158 (w), 1122 (w), 1018 (w), 946 (w), 891 (w), 838 (m), 818 (m), 750 (vs), 695 (w), 659 (m) cm^{-1}.

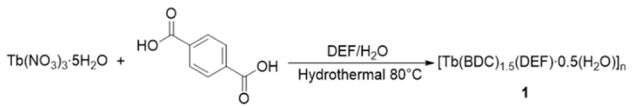

Scheme 1 Synthesis of **1** by a one-step self-assembly process.

Detection of pesticides

Different concentrations of TMX were added to the aqueous solution of compound **1** (20 μg mL^{-1}). After the solution was incubated for 1 min, changes in the emission intensities of the resulting solution were obtained with the emission spectrophotometer (JASCO FP-8300). For the selectivity test, pesticides such as chlorobenzene (CB), carbofuran (CBF), 2,4-dichlorophenol (DCP), carbaryl (CBL), bisphenol A (BPA), 2,6-dichloro-4-nitroaniline (DCN), atrazine (ATZ), and methyl paraben (MPB) with equivalent concentrations of 120 μM were added to the aqueous solution of compound **1**, respectively. Then, emission spectra of the resulting solution were recorded under excitation at 240 nm.

Results and discussion

Synthesis of Tb-MOFs and thermal stability analysis

Compound **1** was synthesized successfully under hydrothermal conditions. Careful control of the cooling period is essential to obtain high quality crystalline products. The purity of the bulk crystalline products of compound **1** was confirmed by powder X-ray diffraction (PXRD) analysis (Fig. 1a). In addition, thermogravimetric analyses from 30 to 950 °C were performed on **1** (Fig. 1b). The continuous weight loss of 18.6% for **1** was in good agreement with the release of one coordinated DEF molecule and one half of a guest water molecule per formula weight before 500 °C (calculated percent weight loss: 21.6% for compound **1**).

Description of crystal structure of 1

A single crystal X-ray diffraction analysis revealed that the solid-state structure of compound **1** crystallizes in a space group *C*2/*c* of a monoclinic unit cell and exhibits a three-dimensional framework structure. In compound **1**, the crystallographic asymmetric unit contains one Tb^{3+} cation, 1.5 BDC^{2-} ligands, one coordinated DEF molecule, and 0.5 guest water molecule with the formula of $[Tb(BDC)_{1.5}(DEF)\cdot 0.5H_2O]_n$ All of the carboxyl groups of the H_2BDC ligands are fully deprotonated, thus achieving charge neutrality with the Tb^{3+} cation. As shown in Fig. 2a, two crystallographically distinct BDC^{2-} ligands present diverse metal–ligand bridging coordination modes. For compound **1**, the Tb^{3+} cation presents in an *octa*-coordination environment (TbO_8) (Fig. 2b); it is coordinated by seven oxygen atoms from six monodentate carboxylate groups as well as one

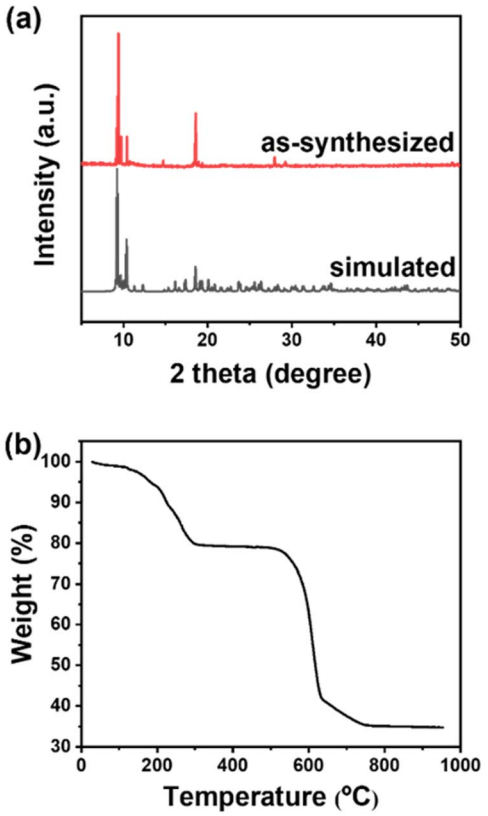

Fig. 1 (a) The PXRD pattern and (b) the thermogravimetric analysis diagram of compound **1**.

chelating carboxylate group, and one monodentate oxygen atom of DEF molecule. Two TbO_8 polyhedrals are bridged by four –COO^- groups to form a Tb_2 dinuclear motif, which is further linked by two additional carboxylate groups to form a rod-shaped Tb-carboxylate chain (Fig. 2c). These Tb-carboxylate chains are linked by the BDC ligands towards a three-dimensional network (Fig. 2d). The rhomboid channels along the crystallographic [001] direction can be observed (Fig. 2d); they are occupied by the coordinated DEF molecules as well as guest water molecules. Several lanthanide compounds with an isostructural network have been reported.[43–46]

The emission property and water stability of the compound 1

The emission spectrum of **1** was measured under an excitation wavelength of 245 nm, and exhibited four characteristic emission peaks at 489, 545, 585, and 621 nm as shown in Fig. 3a. These four peaks corresponded to transitions of $^5D_4 \rightarrow {}^7F_{J=6-3}$ in Tb^{3+} ions, respectively. The stability of the emission intensity of **1** with the time change was also evaluated, which showed that the emission intensity could be maintained at a minimum of 90% after storage in deionized water for five months (Fig. 3b). In addition, compound **1** was investigated *via* immersion in deionized water for at least ten days and then compound **1** showed stable framework structure as revealed from its PXRD patterns (Fig. S1†). Table 1 lists the water stability of Tb-MOFs with different ligands or structures based on PXRD and photoluminescence (PL) detection for comparison.[18,47–55] More significantly, our compound **1** revealed excellent stability in its emission intensity in water for a long period of time, which was exceptional as compared to previously reported Tb-MOFs as shown in Fig. 3c. According to the literature,[56] it is speculated that the formation of strong coordination of the Tb-carboxylate cluster chain unit within the network structure of **1** might facilitate the framework stability of **1** in the aqueous phase.

Sensing pesticides in water

Since compound **1** has the advantage of high stability in water, it was worthwhile to develop further applications in aqueous solution. The emission of compound **1** could be efficiently quenched in the presence of TMX. The quenching process occurred about 10 s after TMX was added to the aqueous solution of compound **1**, as shown graphically in Fig. S2.† Additionally, Fig. 4a shows that the emission quenching of the compound **1** was highly dependent on the concentration of TMX and successive decrements in emission intensity were observed with gradually increasing concentrations of TMX. In Fig. 4b, the quenching trend followed a nonlinear Stern–Volmer

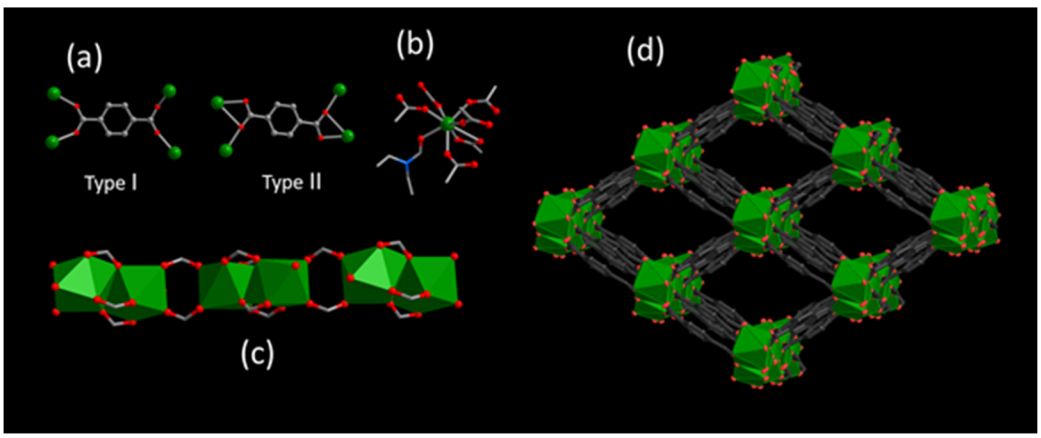

Fig. 2 (a) The ligand bridging modes of BDC^{2-} ligands; (b) the coordination environment of Tb^{3+} cation; (c) the rod-shaped Tb-carboxylate chain; (d) the three-dimensional framework of compound **1**.

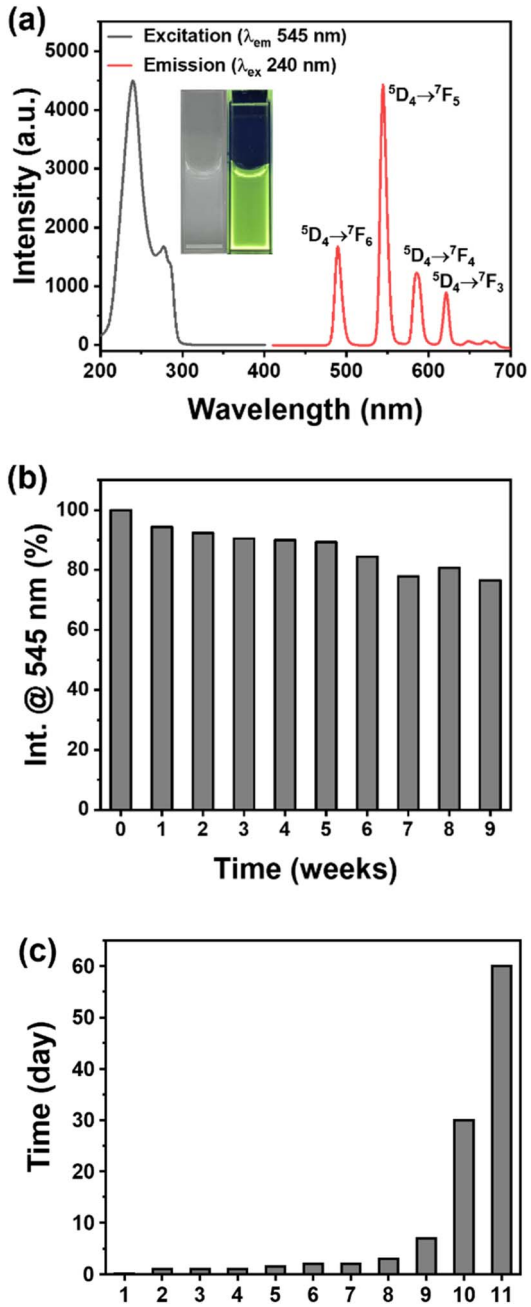

Fig. 3 (a) The excitation and emission spectra and (b) the water stability of compound **1**. (c) Comparison of the water stability of various Tb-MOFs listed in the main text of Table 1.

plot with an upward curvature (*i.e.*, the black squares in Fig. 4b) after introduction of TMX. This indicated that a complex quenching process included both collision and complex formation with the quencher (*i.e.*, TMX). According to the modified Stern–Volmer equation presented as eqn (1),[57] the upward curvature could be well fitted to a linear plot (R^2 = 0.998), the red dots in Fig. 4b, and then analyzed in terms of the dynamic and static quenching constants as shown below:

$$\frac{I_0}{I\exp^{V[Q]}} = 1 + K_{SV}[Q] \quad (1)$$

where I_0 and I are the emission intensities in the absence and presence of TMX, respectively; [Q] is the concentration of TMX (*i.e.*, quencher); V and K_{SV} are the static and dynamic quenching constants, respectively. Accordingly, the static quenching constant (V value) was estimated to be ≈9.2 mM^{-1}, and the collisional (*i.e.*, dynamic) quenching constant (K_{SV} value) yielded nearly 16.42 mM^{-1}. As shown in Fig. S3,† the emission lifetime of compound **1** (~430.4 μs) was slightly decreased after the addition of 100 μM TMX (lifetime ~393.0 μs), indicating that dynamic quenching was indeed involved in the quenching process between the compound **1** and TMX. As for the static quenching, this implied that compound **1** and TMX might generate a non-emissive complex during their encounter. However, the absorption spectra of **1** showed no evident changes after the addition of TMX. Since the zeta potential of compound **1** in deionized water was about +11.39 mV (Fig. S4†) and the pK_a of TMX was ~3.0,[58] it is likely that an electrostatic interaction exists between **1** and TMX in water. These observations indicated that the photoluminescence quenching of compound **1** by TMX could be significantly enhanced only when the electrostatic pair was formed.

The inner filter effect (*i.e.*, competition absorption) refers to the emission quench of **1** by TMX due to the absorption spectrum of TMX exactly overlapping with the excitation spectrum of compound **1** (Fig. S5†). Through this process, the absorption of excitation light by TMX decreases the available energy for compound **1**, resulting in diminishment of the excited state population and subsequent photoluminescence quenching of **1**. This mechanism has been commonly used in sensing Fe^{3+} ions,[59,60] biomolecules,[61,62] and several kinds of pesticides.[48,63] Our compound **1** can be applied to detection of TMX due to its excellent water stability and an appropriate excitation wavelength.

To explore the pesticide sensing capability of compound **1** in water, several different types of pesticides were selected, including chlorobenzene (CB), carbofuran (CBF), 2,4-dichlorophenol (DCP), carbaryl (CBL), bisphenol A (BPA), 2,6-dichloro-4-nitroaniline (DCN), atrazine (ATZ) and methyl paraben (MPB). As shown in Fig. 4c, compound **1** was monitored for its emission at 545 nm upon the addition of various pesticides, respectively. This verified that the luminescent method of compound **1** could selectively detect TMX against other pesticides. By taking advantage of this selectivity, the emission response of compound **1** could be developed as a luminescent probe for detecting TMX. The feasibility of TMX detection was validated as shown in Fig. 4d. The linear calibration curve for determining TMX was obtained by plotting the values of emission intensity ratio (I_0/I) *versus* the concentrations of TMX in the range of 0–40 μM (see Fig. 4d inset), with the calibration curve of $y = 0.03441x + 0.97345$. The limit of detection (LOD) for TMX was determined as 30 nM using the equation LOD = $3\sigma/s$, where σ is the standard deviation and s represents the slope of the calibration.[34] The corresponding detection limit was 30 nM, which is listed in Table S2† for comparison.[41,64–67] Therefore, our results demonstrated that compound **1**, having high water stability, is applicable to the selective sensing of TMX based on luminescence quenching in aqueous solution.

Table 1 Comparison of the water stability of various Tb-MOFs with different ligands or structures

No.	Type	Storage time	Ref.
1	$[Tb_3(dcpcpt)_3(HCOO)]\cdot DMF\cdot 15H_2O$[a]	30 min	47
2	$[Tb_2(H_2btec)(btec)(H_2O)]\cdot 4H_2O$[a]	24 h	48
3	Tb-pek-MOF-1[a]	24 h	49
4	$[(CH_3)_2NH_2]_2[Tb_6(m_3\text{-}OH)_8(FTZB)_6(H_2O)_6]\cdot(H_2O)_{22}$[a]	24 h	50
5	$\{[Tb(CA)(OA)_{0.5}(H_2O)_2]\cdot H_2O\}_n$[a]	36 h	51
6	$Tb^{3+}@Zr_6O_4(OH)_4(O_2C\text{–}C_6H_2\text{–}CO_2(CO_2H)_2)\ xH_2O$[a b]	48 h	52
7	$[Tb_3(H_4L)_2(HCOO)(H_2O)_5]\cdot 14H_2O$[a]	48 h	53
8	$[Tb(TATAB)(H_2O)]\cdot 2H_2O$[a]	72 h	54
9	$\{[Tb(HL)(H_2O)_2]\cdot x(solv)\}_n$[a]	7 days	18
10	$\{[Tb_2(HICA)(BTEC)(H_2O)_2]\cdot 2.5H_2O\}_n$[a b]	30 days	55
11	$[Tb(BDC)_{1.5}(DEF)\cdot 0.5(H_2O)]_n$[a b]	60 days	This work

[a] PXRD: powder X-ray diffraction. [b] No. 6: PL > 95%; no. 10 and 11: PL > 80%.

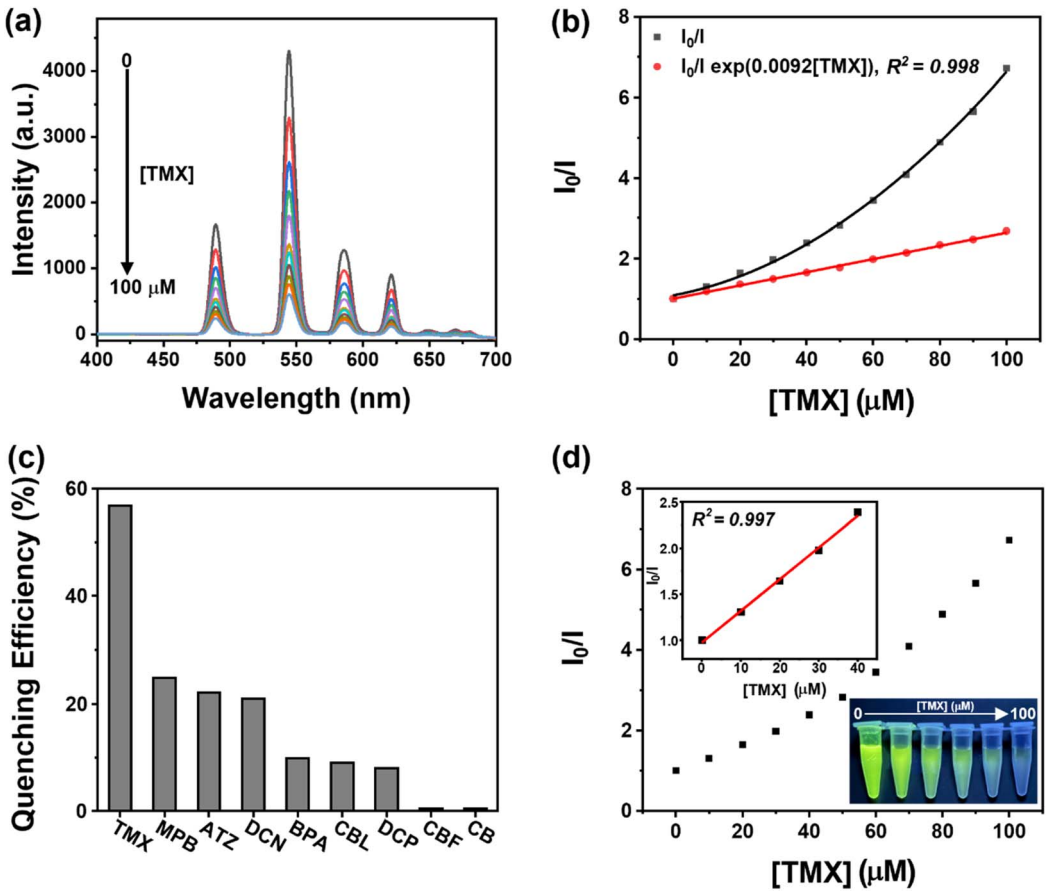

Fig. 4 (a) Changes in the emission spectra of Tb-MOFs with increasing concentrations of TMX were measured at the excitation wavelength of 240 nm. (b) The emission quenching of compound **1** by the addition of TMX was fitted as a nonlinear Stern–Volmer plot (black line) and a modified Stern–Volmer plot (red line), respectively. I_0 and I are the emission intensities of **1** in the absence and presence of TMX, respectively. (c) Changes in the relative emission intensity (at 545 nm) of compound **1** in the presence of various pesticides with equivalent concentrations (40 μM). (d) Changes in emission intensity and the linear relationship (inset) between the intensity of compound **1** at 545 nm and the concentrations of TMX.

Conclusions

In this work, compound **1** was prepared by hydrothermal reactions of 1,4-benzenedicarboxylic acid with the corresponding rare earth ions of Tb^{3+}. Impressively, water stability surveys of compound **1** revealed that it retained ~90% of its emission intensity for five months. With an upward curving Stern–Volmer plot, the green emission of compound **1** quenched by TMX was shown to include both the static and dynamic quenching processes. The quenching mechanism is speculated to involve

the inner filter effect, which is predominantly based on the complete overlap between the absorption spectrum of TMX and the excitation spectrum of **1**. In addition, the quenching efficiency of compound **1** by TMX could be significantly enhanced when the electrostatic pair was formed. Finally, compound **1**, having high water stability, is applicable to the selective sensing of TMX based on luminescence quenching in aqueous solution.

Data availability

The authors declare that the data supporting the findings of this study are available within the paper and its ESI file.† Should any raw data files be needed in another format they are available from the corresponding author upon reasonable request.

Conflicts of interest

There are no conflicts of interest to declare.

Acknowledgements

We gratefully acknowledge Academia Sinica and the National Science and Technology Council (NSTC) of Taiwan (grant number: NSTC 113-2113-M-030-002, NSTC 113-2113-M-030-013, NSTC 113-2740-M-002-007, XRD000200) for providing financial support. We also express our gratitude to Mr Ting-Shen Kuo, National Taiwan Normal University for assistance with the X-ray structure analyses. Special thanks go to Dr Hsien-Ming Lee for his assistance on measurements of zeta potential.

References

1 T. Gorai, W. Schmitt and T. Gunnlaugsson, *Dalton Trans.*, 2021, **50**, 770–784.
2 Y. Zhang, S. Liu, Z.-S. Zhao, Z. Wang, R. Zhang, L. Liu and Z.-B. Han, *Inorg. Chem. Front.*, 2021, **8**, 590–619.
3 M. Sato, T. Ishigaki, M. Iwaki, K. Uematsu, M. Watanabe and K. Toda, *Inorg. Chem.*, 2021, **60**, 17810–17823.
4 Y. Yang, S. Xu, Y. Gai, B. Zhang and L. Chen, *J. Struct. Chem.*, 2022, **41**, 2211045–2211070.
5 L. Duan, C. Zhang, P. Cen, X. Jin, C. Liang, J. Yang and X. Liu, *CrystEngComm*, 2020, **22**, 1695–1704.
6 X.-Z. Xie, Y.-R. Zhang, Y.-J. Wu, X.-B. Yin and Y. Xia, *J. Phys. Chem. C*, 2023, **127**, 1220–1228.
7 T. Yan, Y. Huo and W.-G. Pan, *ACS Appl. Nano Mater.*, 2023, **6**, 10903–10924.
8 P. Ghosh, T. Maity, N. Khatun, R. Debnath and S. Koner, *Polyhedron*, 2022, **219**, 115789.
9 Z. Li, X.-B. Li, M. E. Light, A. E. Carrillo, A. Arauzo, M. Valvidares, C. Roscini, F. Teixidor, C. Viñas, F. Gándara, E. Bartolomé and J. G. Planas, *Adv. Funct. Mater.*, 2023, **33**, 2307369.
10 V. V. Sravani, S. K. Gupta, B. Sreenivasulu, P. Gangopadhyay, C. V. S. B. Rao, A. Suresh and N. Sivaraman, *Opt. Mater.*, 2022, **133**, 112944.
11 L.-L. Ma, G.-P. Yang, G.-P. Li, P.-F. Zhang, J. Jin, Y. Wang, J.-M. Wang and Y.-Y. Wang, *Inorg. Chem. Front.*, 2021, **8**(2), 329–338.
12 Y. Zhao, H. Zeng, X.-W. Zhu, W. Lu and D. Li, *Chem. Soc. Rev.*, 2021, **50**, 4484–4513.
13 S. Wang, B. Sun, Z. Su, G. Hong, X. Li, Y. Liu, Q. Pan and J. Sun, *Inorg. Chem. Front.*, 2022, **9**, 3259–3266.
14 L. Shi, N. Li, D. Wang, M. Fan, S. Zhang and Z. Gong, *TrAC, Trends Anal. Chem.*, 2021, **134**, 116131.
15 X. Wang, K. Batra, G. Clavier, G. Maurin, B. Ding, A. Tissot and C. Serre, *Chem.–Eur. J.*, 2023, **29**, e202203136.
16 Y. Zhao, H. Zeng, K. Wu, D. Luo, X.-W. Zhu, W. Lu and D. Li, *J. Mater. Chem. C*, 2020, **8**, 4385–4391.
17 J. Xiao, L. Song, M. Liu, X. Wang and Z. Liu, *Inorg. Chem.*, 2020, **59**, 6390–6397.
18 M. Lei, F. Ge, X. Gao, Z. Shi and H. Zheng, *Inorg. Chem.*, 2021, **60**, 10513–10521.
19 H. Fu, P. Tan, R. Wang, S. Li, H. Liu, Y. Yang and Z. Wu, *J. Hazard. Mater.*, 2022, **424**, 127494.
20 K.-L. Li, W.-Y. Chen, M. Zhang, X.-W. Luo, Y. Liu, D.-Y. Zhang and A. Chen, *J. Sci. Food Agric.*, 2022, **102**, 417–424.
21 A. R. B. S. Galaco, L. T. Jesus, R. O. Freire, M. de Oliveira and O. A. Serra, *J. Agric. Food Chem.*, 2020, **68**, 9664–9672.
22 T. Wiwasuku, J. Boonmak, R. Burakham, S. Hadsadee, S. Jungsuttiwong, S. Bureekaew, V. Promarak and S. Youngme, *Inorg. Chem. Front.*, 2021, **8**, 977–988.
23 Y. Qiang, W. Yang, X. Zhang, X. Luo, W. Tang, T. Yue and Z. Li, *Microchim. Acta*, 2022, **189**, 130.
24 X. Luo, G. Huang, Y. Li, J. Guo, X. Chen, Y. Tan, W. Tang and Z. Li, *Appl. Surf. Sci.*, 2022, **602**, 154368.
25 Y. Zhang, Y. Liu, P. G. Karmaker, L. Zhang, K. Yang, L. Chen and X. Yang, *ACS Appl. Mater. Interfaces*, 2023, **15**(4), 6177–6186.
26 X.-Y. Guo, Z.-P. Dong, F. Zhao, Z.-L. Liu and Y.-Q. Wang, *New J. Chem.*, 2019, **43**, 2353–2361.
27 Y. Liu, Y. Zhang, P. G. Karmaker, Y. Tang, L. Zhang, F. Huo, Y. Wang and X. Yang, *ACS Appl. Mater. Interfaces*, 2022, **14**, 51531–51544.
28 R. Zheng, Y. Zhang, G. Bao, P. Wu, W. Wei, X. Yuan, T. Zou, T. Zhang and J. Wang, *ACS Sustain. Chem. Eng.*, 2023, **11**, 9077–9086.
29 R. Yousefi, S. Asgari, A. B. Dehkordi, G. M. Ziarani, A. Badiei, F. Mohajer, R. S. Varma and S. Iravani, *Environ. Res.*, 2023, **226**, 115664.
30 S. Liu, J. Zhou, X. Yuan, J. Xiong, M.-H. Zong, X. Wu and W.-Y. Lou, *Food Chem.*, 2024, **432**, 137272.
31 Z. Zhang, L. Zhang, P. Han and Q. Liu, *Microchim. Acta*, 2022, **189**, 438.
32 S. N. Nangare, S. R. Patel, A. G. Patil, Z. G. Khan, P. K. Deshmukh, R. S. Tade, M. R. Mahajan, S. B. Bari and P. O. Patil, *J. Nanostruct. Chem.*, 2022, **12**, 729–764.
33 J. Zhang, W. Zhou, L. Zhai, X. Niu and T. Hu, *CrystEngComm*, 2020, **22**, 1050–1056.
34 X. Xu, Y. Guo, X. Wang, W. Li, P. Qi, Z. Wang, X. Wang, S. Gunasekaran and Q. Wang, *Sens. Actuators, B*, 2018, **260**, 339–345.

35 L. Zhang, Y. Sun, Z. Zhang, Y. Shen, Y. Li, T. Ma, Q. Zhang, Y. Ying and Y. Fu, *Biosens. Bioelectron.*, 2022, **216**, 114659.
36 L. Yang, Y.-L. Liu, C.-G. Liu, F. Ye and Y. Fu, *Inorg. Chem. Commun.*, 2020, **122**, 108272.
37 Z.-D. Zhou, C.-Y. Wang, G.-S. Zhu, B. Du, B.-Y. Yu and C.-C. Wang, *J. Mol. Struct.*, 2022, **1251**, 132009.
38 X. Chen, Y. Li, J. Li, L. Cao and C. Yao, *Anal. Methods*, 2023, **15**, 2946–2954.
39 W. Wang, F. Yang, Y. Yang, Y.-Y. Wang and B. Liu, *J. Agric. Food Chem.*, 2022, **70**, 15682–15692.
40 A. Li, Q. Chu, H. Zhou, Z. Yang, B. Liu and J. Zhang, *Inorg. Chem. Front.*, 2021, **8**, 2341–2348.
41 R. Cui, R. Li, Z. Li, M. Wei, X. Wang and X. Li, *Dyes Pigm.*, 2021, **195**, 109669.
42 Y. Xu, X. Li, W. Zhang, H. Jiang, Y. Pu, J. Cao and W. Jiang, *Food Chem.*, 2021, **344**, 128650.
43 J. P. Vizuet, A. L. Lewis, G. T. Mccandless and K. J. Balkus, *Polyhedron*, 2021, **205**, 115283.
44 M. Kariem, M. Yawer, S. Sharma and H. N. Sheikh, *ChemistrySelect*, 2016, **1**, 4489–4501.
45 H. F. Clausen, J. Overgaard, R. D. Poulsen, W. Morgenroth and B. B. Iversen, *Acta Crystallogr., Sect. E: Struct. Rep. Online*, 2006, **62**, m3333–m3335.
46 R. D. Poulsen, J. Overgaard, M.-A. Chevalier, H. F. Clausen and B. B. Iverson, *Acta Crystallogr., Sect. E: Struct. Rep. Online*, 2005, **61**, 1337–1339.
47 M. Yu, Y. Xie, X. Wang, Y. Li and G. Li, *ACS Appl. Mater. Interfaces*, 2019, **11**, 21201–21210.
48 T. Wiwasuku, A. Chuaephon, U. Habarakada, J. Boonmak, T. Puangmali, F. Kielar, D. J. Harding and S. Youngme, *ACS Sustainable Chem. Eng.*, 2022, **10**, 2761–2771.
49 D. Alezi, A. M. Peedikakkal, Ł. J. Weseliński, V. Guillerm, Y. Belmabkhout, A. J. Cairns, Z. Chen, Ł. Wojtas and M. Eddaoudi, *J. Am. Chem. Soc.*, 2015, **137**, 5421–5430.
50 D.-X. Xue, A. J. Cairns, Y. Belmabkhout, L. Wojtas, Y. Liu, M. H. Alkordi and M. Eddaoudi, *J. Am. Chem. Soc.*, 2013, **135**, 7660–7667.
51 H. Min, Z. Han, M. Wang, Y. Li, T. Zhou, W. Shi and P. Cheng, *Inorg. Chem. Front.*, 2020, **7**, 3379–3385.
52 K. Ge, X. He, Z. Xu and R. Chu, *ChemistrySelect*, 2019, **4**, 12573–12579.
53 L. Chen, C.-L. Wang, C.-Y. Zhu, P. Li, W. Gao, J.-Y. Li and X.-M. Zhang, *J. Solid State Chem.*, 2022, **314**, 123423.
54 J.-H. Wei, J.-W. Yi, M.-L. Han, B. Li, S. Liu, Y.-P. Wu, L.-F. Ma and D.-S. Li, *Chem.–Asian J.*, 2019, **14**, 3694–3701.
55 H. Yu, M. Fan, Q. Liu, Z. Su, X. Li, Q. Pan and X. Hu, *Inorg. Chem.*, 2020, **59**, 2005–2010.
56 C. Xiao, J. Tian, Q. Chen and M. Hong, *Chem. Sci.*, 2024, **15**, 1570–1610.
57 T.-H. Wu, Y.-Y. Hsu and S.-Y. Lin, *Small*, 2012, **8**, 2099–2105.
58 C. F. Silva, L. F. Menezes, A. C. Pereira and C. S. Nascimento, *J. Mol. Struct.*, 2021, **1231**, 129980.
59 C.-Y. Zhu, M.-T. Shen, H.-M. Cao, M.-J. Qi, P. Li, L. Chen, Y. Ge, W. Gao and X.-M. Zhang, *Microchem. J.*, 2023, **188**, 108442.
60 H. Yu, Q. Liu, J. Li, Z.-M. Su, X. Li, X. Wang, J. Sun, C. Zhou and X. Hu, *J. Mater. Chem. C*, 2021, **9**, 562–568.
61 J. Xu, H. Zhang, W. Zhang, P. Li, W. Zhang, H. Wang and B. Tang, *Chem. Commun.*, 2020, **56**, 2431–2434.
62 C. Guo, Q. Jin, Y. Wang, B. Ding, Y. Li, J. Huo and X. Zhao, *Sens. Actuators, B*, 2016, **234**, 184–191.
63 G. Qin, Y. Kong, T. Gan and Y. Ni, *Inorg. Chem.*, 2022, **61**, 8966–8975.
64 E. J. Llorent-Martínez, M. I. Soler-Gallardo and A. Ruiz-Medina, *Luminescence*, 2019, **34**, 460–464.
65 J. Jiménez-López, P. Ortega-Barrales and A. Ruiz-Medina, *Talanta*, 2016, **149**, 149–155.
66 Y. Dai, W. Xu, J. Hong, Y. Zheng, H. Fan, J. Zhang, J. Fei, W. Zhu and J. Hong, *Biosens. Bioelectron.*, 2023, **238**, 115559.
67 X. Fang, D. Duan, J. Ye and K. Li, *Anal. Chim. Acta*, 2021, **1183**, 338938.